ANALYSIS OF STEEL-CONCRETE COMPOSITE BOX GIRDER BRIDGES WITH EXTERNAL PRESTRESSING

Bruno Tasca de Linhares

bruno.linhares@unochapeco.edu.br

Universidade Comunitária da Região de Chapecó (Unochapecó)

Avenida Senador Attilio Fontana 591E, 89809-000, Santa Catarina, Chapecó, Brazil

Abstract. *Steel-Concrete Composite Structures have been used in the construction of bridges and urban viaducts, especially from the second half of the twentieth century. This is due to its high flexural capacity and torsion stiffness. Grounded in the American Standard AASHTO-LRFD:2012 and the literature review, it is proposed a case study for analytical verification of a composite structure, concerning positive and negative bending moments, shear and shear connectors. After this initial stage, prestressing was applied to the structure, and with analytical methods and the virtual work method, the ratio between the additional strain of the tendons and the external applied moment were obtained. Thus, it was possible to make the horizontal plastic forces balance through the Bisection Method to obtain the increment of positive and negative flexion strength. It was observed with prestressing, an important increase of capacity in the negative bending region for ULS (~40%); for the positive bending region, the increase was somewhat higher than 7%. Finally, a finite element model with shell elements was held with the software SAP2000 to confront the initial analysis. The results show that the initial space frame bars model, in terms of displacements and stresses, is appropriate to analyze this type of structure.*

Keywords: *composite structures; box girder; external prestressing; virtual work method; prestressing losses.*

INTRODUCTION

The systems with mixed structures for bridges aim to combine steel and concrete in order to obtain the maximum efficiency of both materials. Composite structures were introduced at in the post-World War II period and have been, in the last five decades, one of the most suitable and versatile systems for the use of composite materials in highway applications.

The first mixed elements used were the beams; the steel beams were involved with concrete without structural function in order to increase the resistance to fire, but with the development of bigger resistances for the concrete, it came to be taken into account in the resistance of the set.

According to De Nardin and Souza (2008), the use of composite steel-concrete elements enlarges the set of solutions in reinforced concrete and steel. The spreading of composite structures is due to factors such as: transparency of the structure, reduction of cross-sectional, smaller weight, faster and easier execution and reduced costs with materials and manpower.

The composite action not only reduces the stresses of the variable loads, but also the deflections due to the increase in flexural stiffness. This is ensured by the presence of the shear connectors attached to the beam. Mixed sections and types of connectors are shown in Figs. 1 to 3, but the flexible connectors, or Stud Bolts, have become the most commonly used today and are exemplified in Fig. 4 (KLAIBER; WIPF, 1999).

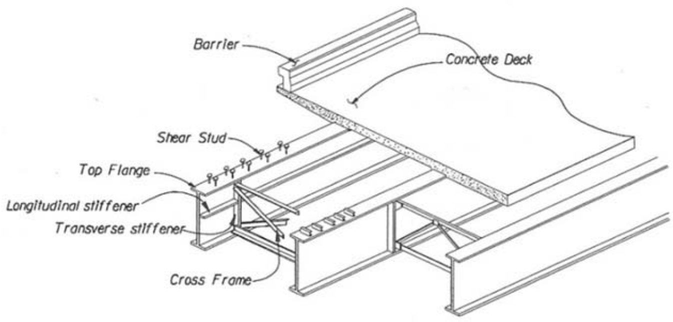

Figure 1. “I” Shape Plate Girder (DUAN et al., 1999)

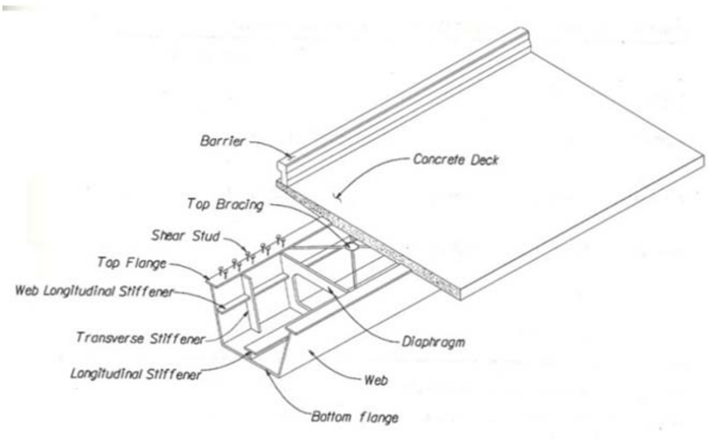

Figure 2. Composite Box Girder (SALEH; DUAN, 1999)

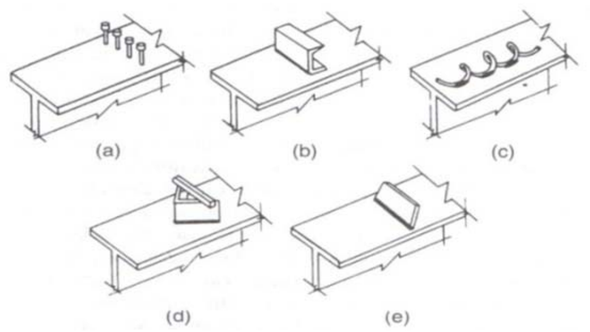

Figure 3. (a) Welded Stud Bolts; (b) Bar Channel Connector; (c) Spiral Connector; (d) Stiffened Angle; (e) Inclined plate (KLAIBER; WIPF, 1999)

Figure 4. Welded Shear Connector Stud Bolts

Composite beams can also be defined with prefabricated concrete slabs. The use of prefabricated slabs is a quick solution with the advantage of dispensing formworks. Prefabricated panels receive holes or shear pockets directly at Stud Bolts positions in the structural steel. The welded connectors are then positioned through the shear pockets in the slab. The composite action will be ensured by filling the pockets as well as the joints between the panels and the steel beams with quick curing concrete and low shrinkage (Figs. 5 and 6).

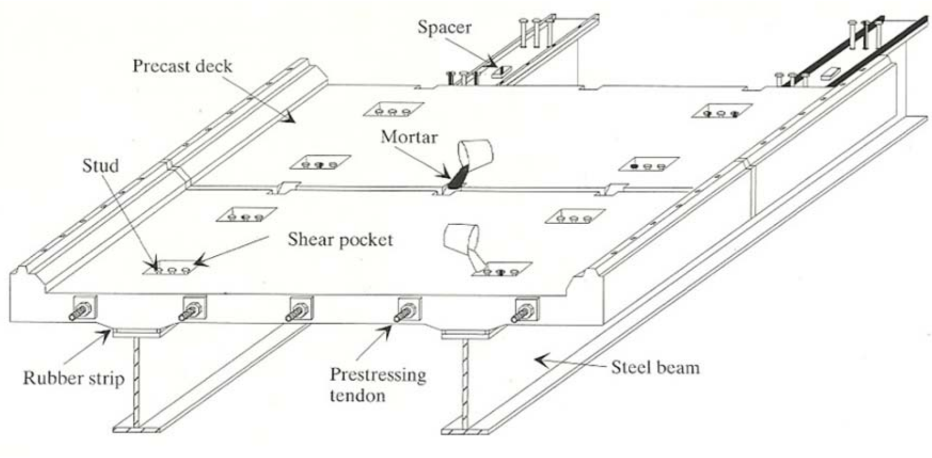

Figure 5. Shear Pockets and Grouting of the Joints (SHIM et al., 2010)

Figure 6. Shear Pockets of Prefabricated Concrete Slabs

Bridges and viaducts designed from old standards suffer gradual deterioration due to current traffic loads. In general, the reinforcement of the structure with the application of external prestressing is an economical and efficient alternative to the implantation of a new structure. The advantages of this technique are: to extend the elastic behavior of the bridge, to increase its ultimate capacity, to increase the capacity to fatigue and to reduce displacements.

External prestressing can also be used to convert an isostatic structure into a hyperstatic structure, as it develops continuity. Since the 1950s, external prestressing has been used to reinforce steel girders and trusses, box concrete sections and mixed bridges. Figure 7 illustrates some configurations of external cables, which can be applied in both concrete and steel and / or mixed sections.

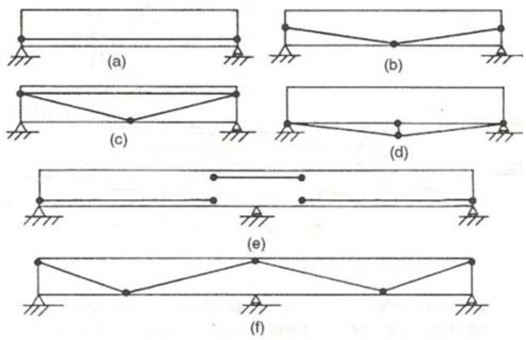

Figure 7. Tendon Configurations for External Prestressing (KLAIBER; WIPF, 1999)

Due to the lack of Brazilian Standardization and scarcity of national materials, it is necessary to study the calculation procedures/selection of mixed structures for bridges/viadutcs. Box Girder Bridges have great advantages for roadworks: efficiency, quick construction, great load capacity and little interference with the environment.

The study of the prestressing is important for this type of structure whereas the growth of national development tends to increase the volume of traffic submitting the structures to load excesses. A prestressing is an alternative for the attenuation of the effects, in particular to box section girder bridges, due to its hollow cross-section, where it is possible to install the tendons in its interior.

Therefore, the objective of this paper is to propose the study of a case, a continuous tangent composite steel-concrete box girder bridge of 2 spans, to carry out its analytical verification according to the criteria of the AASHTO-LRFD: 2012 standard, to determine its resistance in Ultimate Limit State (ULS) and define shear connectors. Thus, to apply a prestressing force to the structure, which respects its admissible stresses, and to present the method for the verification in ULS with the prestressing. The focus is given especially to the ULS of the negative flexion, in the region of continuity of the spans. The verification of the negative flexion region in composite structures is usually omitted or presented without proper details in technical manuals and books, different approach from the case of positive flexion. Thus, it is intended to construct a method of checking the flexion in the region of negative moment of a composite box girder section with external prestressing and to present the increment of resistance in ULS.

An initial structural analysis is performed using a space frame bars model using the STRAP 2013 software. Finally, a finite-element model with shell elements is performed with SAP2000 software to compare/validate the results of the original model, especially in terms of stresses and displacements. The finite element model with SAP2000 is justified since this software has thin shell and thick shell elements, whereas the STRAP 2013 software provides only thin shell elements.

1 STUDY CASE

It is proposed to study an application case. A cross-section is established. The construction phases of the model, the considerations to take into account these phases, the main loads, and results that will serve as basis for an analytical verification of the structure are presented.

1.1 Cross Section

The following composite box girder section is defined (Fig. 8):

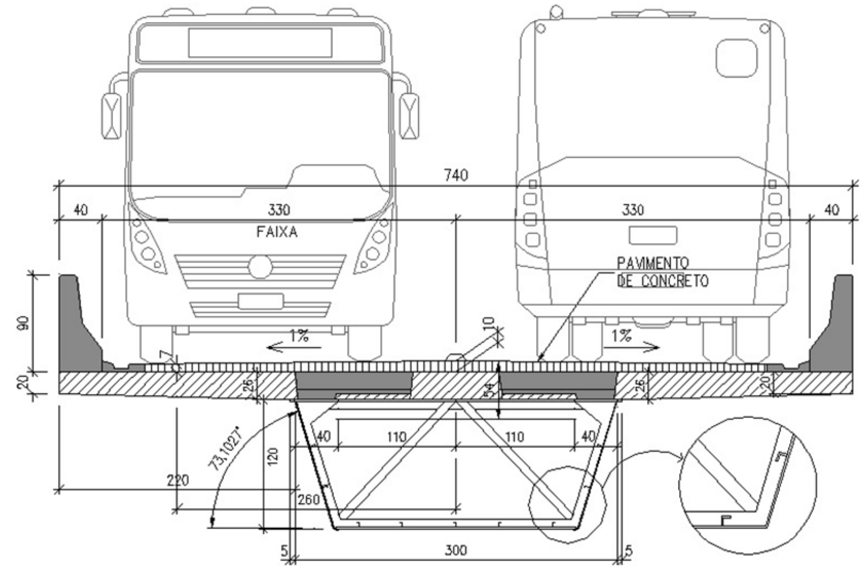

Figure 8. Steel-Concrete Composite Box Girder Case

The structure is formed by two continuous 25m length spans divided into 10 staves of 2.5m length, which are welded to compose the entire piece; therefore, 11 cross sections for calculations. The section is composed of two bands of 3.30m with total 7.40m width. The CORTEN steel box section (F_y = 345MPa) is 1.20m depth and the webs are 73.1027º inclined. The composite plates have variable thickness to meet the maximum flexural and shear stresses (Table 1).

Table 1. Plates Thickness

Plate Thickness	Staves 1 and 2	Staves 3 to 8	Staves 9 and 10
Top Flanges	1”	1”	1”
Webs	3/4”	5/8”	3/4”
Bottom Flanges	1”	1,25”	1”

The concrete slab has an average thickness of 26cm and is cast with concrete f_{ck} = 40MPa. In the cross section (Fig. 8), the longitudinal stiffeners, which are composed of 4"x 4"#3/8" L-shaped plates, are also indicated. Five longitudinal stiffeners are defined in the bottom flanges and two in each web. The internal bracing is made by K-shaped framework with 4"x 4"#3/8" L-shaped plates.

In the central pillar region, a continuity reinforcement of the concrete is composed by 32 16mm diameter bars with 4cm of covering, which corresponds to a total reinforcement area of 64.33cm².

1.2 Structural Model and Analysis

The structure elastic-linear analysis was performed in STRAP 2013 software (Structural Analysis Programs), which is a program that applies the direct stiffness method as well as the finite element method (bars, flat elements and solids). In this study, space frame bar elements were used.

The tangent model with two 25m length spans has three identical 6m height rectangular pillars. In the first and last pillars there are movable bearing supports devices that allow the free longitudinal movement and rotation of the superstructure on these pillars. These supports are Unidirectional Cernoflon (CU) type. In the central pillar, a crimp-fitting (continuous) type connection is considered, since it is foreseen a massive concrete casting inside the steel box section over the central pillar and a continuity reinforcement.

The construction phases should be considered separately, since the geometric properties vary between the analyses; they are: **Isostatic Box Section Phase**, **Hyperstatic Box Section Phase**, **Long Term Composite Section Phase** and **Short Term Composite Section Phase**.

The first one, **Isostatic Box Section Phase,** consists in an isostatic steel box section supporting its own weight (**g1**); its geometric properties do not consider those of the slab concrete (Fig. 9a).

The second phase is the **Hyperstatic Box Section Phase**, in which the steel box section, before isostatic, are now welded together on the central pillar and receive the loads of precast concrete slabs (**g2**), before the shear pockets grouting. Therefore, the structural steel keeps working in isolation, but no longer isostatically (Fig. 9a).

The **Long Term Composite Section Phase** consists of the solidarity between the slabs and the structural steel after the shear pockets grouting. The slab is transformed into a fictitious steel section (homogenization) through the factor 3n (where n is the ratio between the steel modulus of elasticity and concrete one). Its width is divided by this factor. The section already works as a composite structure and receives the remaining dead loads (**g3**). The slab section is now a small fictitious steel area over the steel box section (Fig 9b). The factor 3n (Long Term) occurs due to the concrete creep effect under dead loads.

The last phase, **Short Term Composite Section Phase**, receives the mobile (vehicles) loads, and follows the same process as the previous one, but the section is homogenized by the n-factor only, since these loads are short term loads (Fig. 9c). It is important to note that for the elastic-linear analysis, the standard allows the concrete slab to be used throughout the bridge deck, even under negative flexion in the internal supports. Tests have indicated that neglecting the slab in those negative flexion regions has little effect on the overall elastic behavior of the structure (AASHTO-LRDF: 2012).

All the geometric properties of the phases (moments of inertia, centroids, static moments, areas) were determined by the Green Method implemented in MathCad.

The elastic-linear structure was modeled with de aid of the software STRAP 2013. The load combinations for ULS followed the prescriptions of AASHTO-LRFD: 2012.

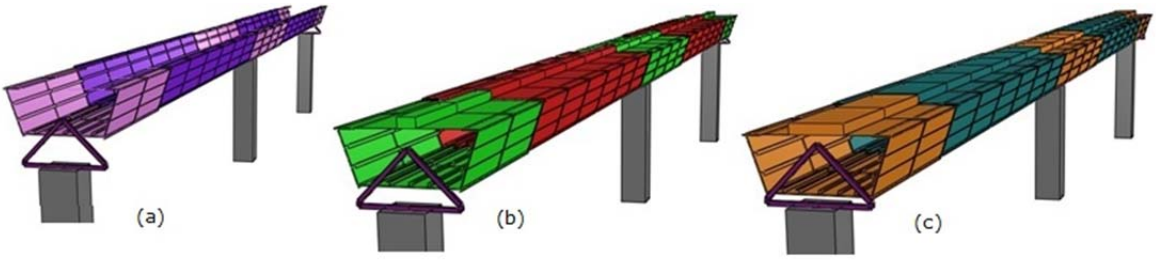

Figure 9. (a) Isostatic and Hyperstatic Box Section Phases; (b) Long Term Composite Section Phase; (c) Short Term Composite Section Phase – STRAP 2013 elastic-linear models

In order to simulate the bearing conditions and the degrees of freedom over the pillars, the rigid triangle elements represented in Fig. 9 are defined. The mobile, dead and live loads, as well as their position in the bridge deck were defined according AASHTO-LRDF: 2012.

1.3 Ultimate Flexural Capacity

According to the AASHTO-LRFD:2012 Standard, the resistant plastification moment is obtained from a balance of plastic forces around the plastic neutral axis (PNA) for positive bending, see Fig. 10. The position of the Plastic Neutral Axis is obtained by plastic forces horizontal equilibrium.

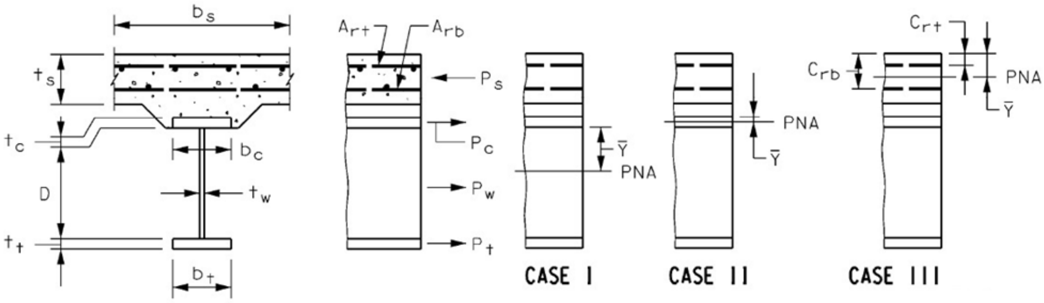

Figure 10. Plastic Forces and Positions of the Plastic Neutral Axis for Positive Bending. Case I: PNA in the web; Case II: PNA in the top flange; Case III: PNA in the concrete slab

In Fig. 10, $P_s = 0.85f_cb_st_s$ (resulting force from the slab, where f_c is the concrete strength and t_s, slab thickness); $P_c = F_yb_ct_c$ (resulting force from the top flange); $P_w = F_yDt_w$ (resulting force from the web); $P_t = F_yb_tt_t$ (resulting force from bottom flange); F_y = steel yielding stress; PNA - Neutral Plastic Axis; A_{rt} and A_{rb} are the upper and lower reinforcement, respectively, of the slab. Finally, the Moment of Plastification is determined by the Eq. (1):

$$.M_p = \sum_{i=1}^{4} F_{P_i} Y_i \tag{1}$$

The Wittry[1] safety criterion (1993 apud AASHTO-LRFD: 2012) is then applied to the theoretical value of the resistant plastification moment.

In the regions of negative bending moment, the calculation of the resistant moment does not involve the moment of plastification of the section, but a limitation of the stresses in both top and bottom flanges.

The geometric properties of the cross section will then be calculated with the steel box section and the negative reinforcement of the slab. The concrete slab will be subject to tensile stresses and therefore is ignored in the calculation (AASHTO-LRFD:2012).

In this case, the bottom flange of the box section is compressed and the top ones are in tensile stresses. The tensile stresses are limited by the steel yielding stress (F_y). The stress at the compressed flanges (F_{nc}) will depend on their slenderness, the presence or absence of longitudinal stiffeners, their slenderness between stiffeners, the tensions of St. Venant. In short: $\sigma_{lim}{}^{sup} = F_y$; $\sigma_{lim}{}^{inf} = F_{nc}$ (AASHTO-LRFD:2012).

It is enough to calculate a minimum bending moment of external load that takes the section under negative moment to reach these stresses. In possession of this bending moment, the three parcels of the sum that define the negative resistant moment of the section are obtained (Eqs. (2) to (4)):

$$.\sigma_{lim}^{inf} = \frac{M_{D1}}{W_{box\,section}^{inf}} + \frac{M_{D2}}{W_{composite}^{inf}} + \frac{M_{AD}{}^{inf}}{W_{composite}^{inf}} \tag{2}$$

$$.\sigma_{lim}^{sup} = \frac{M_{D1}}{W_{box\,section}^{sup}} + \frac{M_{D2}}{W_{composite}^{sup}} + \frac{M_{AD}{}^{sup}}{W_{composite}^{sup}} \tag{3}$$

$$.M_{dres}^{neg} = M_{D1} + M_{D2} + \min(M_{AD}{}^{sup}, M_{AD}{}^{inf}) \tag{4}$$

[1]WITTRY, D. M. **An Analytical Study of the Ductility of Steel Concrete Composite Sections**. Master Thesis. University of Texas, Austin, 1993.

In which:

$\sigma_{lim}{}^{sup}$ - F_y; $\sigma_{lim}{}^{inf}$ - F_{nc}; $M_{dres}{}^{neg}$ = negative resistant bending moment;

M_{D1} - design negative moment for isolated continuous steel box section under loads g1 and g2;

M_{D2} - design negative moment for continuous steel-concrete composite box section under g3;

M_{AD} - mobile loads responsible for making the bottom and top flanges reach the limiting stresses;

1.4 Shear Capacity

The webs ultimate shear strength without transverse stiffeners is given either by shear flow or by shear buckling. The relati on between these two quantities is made by the constant C (AASHTO-LRFD:2012). The shear capacity is given by Eq. (5):

$$.V_n = V_{cr} = CV_p \ \ where\ V_p = \ 0.58F_y.D.t_w \tag{5}$$

In which:

D - web depth;
t_w - web width;
V_p - shear flow resistance;
C - relation between shear flow or by shear buckling (AASHTO-LRFD:2012).

1.5 Shear Connectors

The shear connectors must are calculated to withstand the Fatigue Limit State only.

The shear stresses required to check the connectors result from combinations of fatigue loads. Combinations of fatigue take into account only the traffic loads with their fatigue factors. Since mobile loads are short-duration loads, the shear flow must come from the short term analysis, that is, with the homogenization of the cross-section from n (= E_s / E_c)

The shear flow used for the verification of the connectors comes from the maximum shear amplitude in the section. The shear stress, in an analysis section, can change signal according to the influence line of the moving load. Thus, one should consider the range of shear variation (Eq. 6):

$$.V_f = |+V_M| + |-V_M| \tag{6}$$

The shear fatigue resistance for a shear connector is a function of the number of cycles to which it will be subjected. The number of cycles (N), in turn, is determined by the number of trucks per day in one direction, for 75 years of work life, according to AASHTO-LRFD: 2012.

The fatigue shear flow responsible for the dimensioning of the connectors comes from the torsion and shear stresses represented by the Eq. (7):

$$.p = \frac{N*Z_r}{\sqrt{V_{sr}{}^2+V_{st}{}^2}} \tag{7}$$

In which:

V_{sr} - flow shear from flexure effects;
V_{st} - flow shear from torsion effects;
Z_r - fatigue resistance of one shear connector;
p – connectors pitch.

1.6 Results

Mnom =

	0
0	41076
1	40056
2	39389
3	45433
4	45383
5	45610
6	46113
7	46887
8	-12373
9	-13881
10	-14569

kN·m

Mumax =

	0
0	4910
1	9400
2	12920
3	14370
4	14410
5	13040
6	10320
7	6260
8	-4490
9	-9790
10	-17000

kN·m

Razão =

	0
0	11.95
1	23.47
2	32.8
3	31.63
4	31.75
5	28.59
6	22.38
7	13.35
8	36.29
9	70.53
10	116.68

%

Figure 11. M_{nom} (Nominal Strength Moments); M_{umax} (Design Moments Envelope); Razão (Ratio)

Figure 11 shows the Ultimate Limit State (ELU) combination envelope results for Bending Moments, and Fig. 12, for the Shear Efforts. The vectors exhibit strength and design efforts.

Vn =

	0
0	4616
1	4616
2	4616
3	3454
4	3454
5	3454
6	3454
7	3454
8	4616
9	4616
10	4616

kN

Vualma =

	0
0	1270
1	1085
2	793
3	725
4	631
5	854
6	1108
7	1371
8	1635
9	1921
10	2098

kN

Razão =

	0
0	27.52
1	23.51
2	17.17
3	21
4	18.28
5	24.74
6	32.09
7	39.68
8	35.43
9	41.62
10	45.45

%

Figure 12. V_n (Strength Shear Efforts); V_{ualma} (Design Shear Efforts Envelope); Razão (Ratio)

The ULS condition will be satisfied if the resistive efforts are greater or equal to the ultimate actions. Therefore, these results are compared to the resistances obtained by the analytical calculation. The results were presented only for the first span (symmetrical to the other span).

It can be seen that the majority of the sections meet the efforts in ULS. In regions of negative bending, since the slab did not contribute to section's capacity, the maximum stress exceeded by 16.68% the ultimate strength of the section. This percentage is guaranteed by the presence of the negative reinforcement. In the case of neglecting the negative continuity reinforcement in the central support (32 bars φ16mm), the ratio in this section would be 137.40%, that is, 37.40% beyond the capacity of the section. With this, one can see the importance of the negative continuity reinforcement between continuous spans.

In the case of shear stresses, the webs thickness (3/4 " and 5/8 ") respected the limit slenderness for the compact section and guaranteed the design shears efforts (maximum 45.45% of capacity).

The shear connectors determination by fatigue combinations result in a number of connectors per stave for each web. The bending shear stresses (Vf) and St. Venant´s torsion shear stresses (Tf) for fatigue combinations are shown in Fig. 13.

Vf = (kN)

	0
0	390
1	320
2	300
3	280
4	280
5	300
6	290
7	330
8	390
9	440

Tf = (kN·m)

	0
0	540
1	490
2	440
3	410
4	370
5	400
6	430
7	470
8	520
9	570

Vsr = ($\frac{kN}{m}$)

	0
0	150
1	123
2	113
3	105
4	105
5	113
6	109
7	124
8	150
9	169

Vst = ($\frac{kN}{m}$)

	0
0	77
1	70
2	63
3	59
4	53
5	57
6	62
7	67
8	75
9	82

Bolts =

	0
0	45
1	39
2	36
3	33
4	33
5	36
6	36
7	39
8	45
9	51

Figure 13. V_f (Fatigue Bending Shear Efforts); T_f (Fatigue Torsion Shear Efforts); V_{sr} (Flow Shear of Fatigue Bending Shear Efforts); V_{st} (Flow Shear of Fatigue Torsion Shears Efforts); Bols (Number os Stud Bolts per Stave for each Web)

This Bolts definition will be used in Finite Elements Model.

2 PRESTRESSING

As seen at 1.6 the negative bending region over the central pillar has a final capacity of 16.68% lower than the maximum design negative bending moment. Capacity is increased by the presence of negative continuity reinforcement. In this chapter prestressing is applied to increase the ULS strength for both positive and negative bending moments.

2.1 Prestressing tendons

The development of the tendons was established according to Fig. 14. The dashed line defines the center of gravity (CG) of the Long Term Steel-Concrete Box Girder.

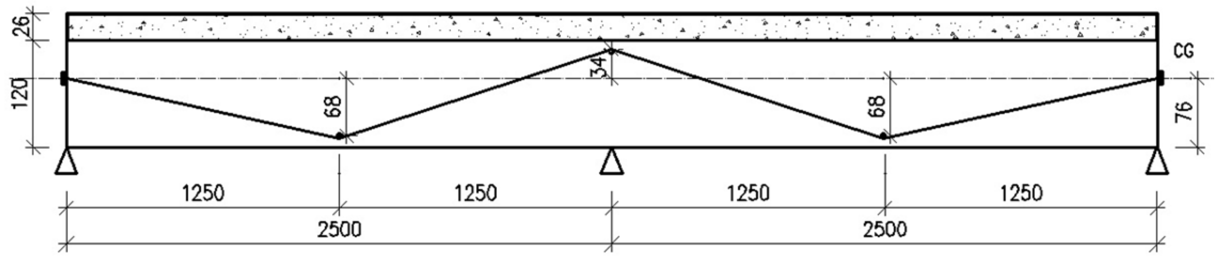

Figure 14. Prestressing Tendons Development [cm]

Limited Prestressing is defined, that is, for frequent loads combinations the concrete cracking limit stress must be respected. Therefore, it is necessary to respect the steel tensile stresses and the maximum compression stresses in the slab. A total force of 1275 tf (12750kN) is defined.

Four tendons of 15 strands (Φ15.2mm; A_p = 140mm^2/strand; strength force = 265,8kN/strand) are used. Each strand consists of a bundle of 7 greased wires wrapped by a high density polyethylene sheath (HDPE). The force per tendon is given by Eqs. (8) and (9):

$$.P_{total} = 4 * \beta * 15 * 26,58 \;\cong 1275 ton;\;\; where\; \beta = 0.8 \tag{8}$$

$$.P_{tendon} = \frac{1275tf}{4} \cong 319 ton \tag{9}$$

A cross section with the tendons location for the study case is shown in Fig. (15).

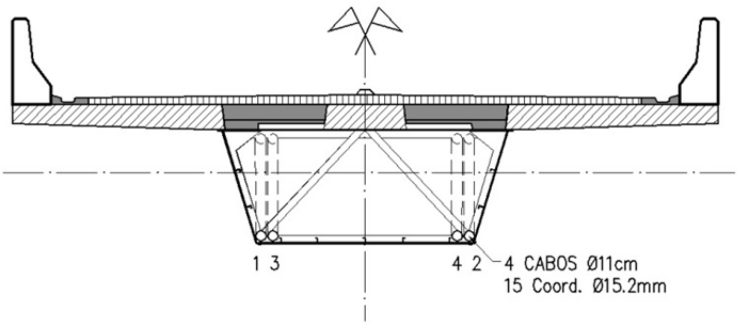

Figure 15. Cross Section with Tendons Location. Trad.: *Cabos* (Tendons); *Coordoalhas* (Strands)

The following data are defined: the 4 tendons are prestressed in two stages (2 tendons at a time); wedge retreat is 5mm (wedge retreat losses); sheath friction coefficient μ = 0,1rad^{-1}; sheath parasite friction coefficient λ = 0,007rad/m.

The prestressing losses are estimated in 15%, based on the work of Nunziata (2004), who estimates losses of 10% for prestressed steel structures. These values will be confronted by calculation.

2.2 Positive Strength Bending Moment

The ULS for the prestressed composite structure in positive bending regions with a compact steel section is characterized by the complete plastification of the sections of the slab and steel beam. The difference in this case is the presence of the prestressing tendons, which will be subjected to its rupture stress (see Fig. 16).

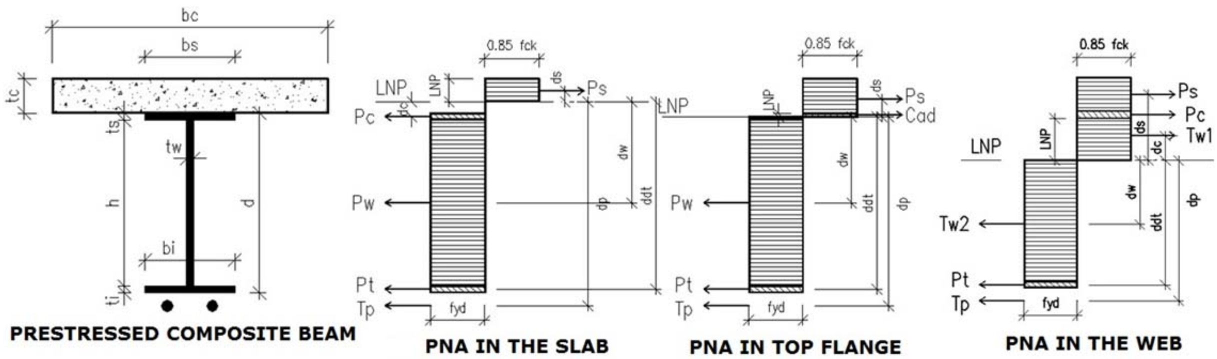

Figure 16. Plastic Forces Horizontal Balance – Positions of the Plastic Neutral Axis (PNA = LNP)

The process consists in determining the position of the Plastic Neutral Axis by the balance of horizontal plastic forces. Once the PNA is determined, the bending moments produced around it are added, which results in the Positive Resistant Bending Moment (see item 1.3).

2.3 Negative Strength Bending Moment

It was verified that the AASHTO-LRFD: 2012 Standard establishes as ULS negative bending moment regions the smallest bending moment between the yielding bending moment on top flange and the compression stress limit on the bottom flange.

By maintaining the same criterion, the smallest bending moment is determined between the two equilibrium situations in ULS shown in the Fig. 17 (the slab is neglected).

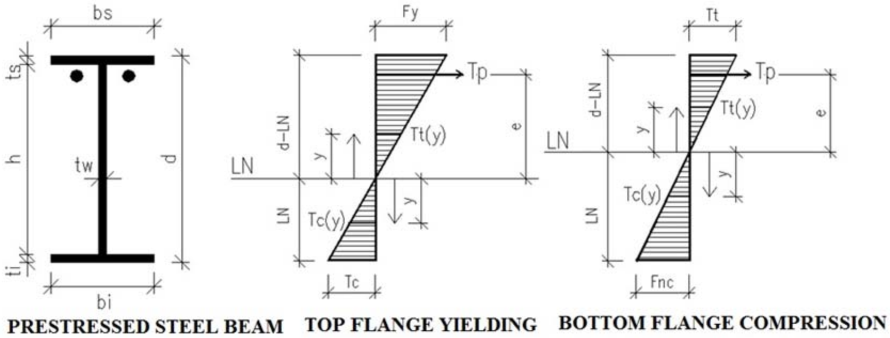

Figure 17. ULS for Prestressed Composite Beam under Negative Bending (LN = Neutral Axis)

The Horizontal Forces Balance is given by Eqs. (10) to (11):

$$.\sum F_H = R_t + T_p - R_c = 0 \quad (10)$$

$$.\int_0^{d-LN} T_t(y).b.dy + \left(F_{p\infty} + \Delta F_p.M_d\right) + \int_0^{LN} T_c(y).b.dy = 0 \quad (11)$$

The sum of Bending Moments around the Elastic Neutral Axis (LN) is determined from Eq. (12):

$$.M_d = \int_0^{d-LN} T_t(y).b.y.dy + \int_0^{LN} T_c(y).b.y.dy + \left(F_{p\infty} + \Delta F_p.M_d\right).e \quad (12)$$

In which:

$F_{p\infty}$ - tendons force with the losses dicounted;
ΔF_p – unitary increase of the prestress force due to the negative moment [kN / kN.m];
M_d – strength bending moment; $F_{p\infty}$ - tendons force with the losses dicounted;
e – prestressing eccentricity in relation to the Elastic Neutral Axis.

By linear stress relations in the Fig. 16, it is possible to obtain:

$$.T_c(LN) = \frac{LN}{d-LN}.F_y \rightarrow compression\ stress\ bottom\ flange \quad (13)$$

$$T_t(LN) = \frac{d-LN}{LN}.F_{nc} \rightarrow yielding\ stress\ top\ flange \quad (14)$$

According to studies by Quinaz (1993) and Choi et al. (2008), the increase of prestressing force in the tendons, or relation between the negative bending moment and the increase of the prestressing tendons deformation, can be obtained with the aid of the virtual works method (VWM). In this way a unitary moment is applied in the region of the central support and a unitary force in the cable. With the VWM, the relationship between this moment and the additional force on the tendons (ΔF_p) is found. It is considered that the inflection point on the central support is indeslocable (Fig. 18).

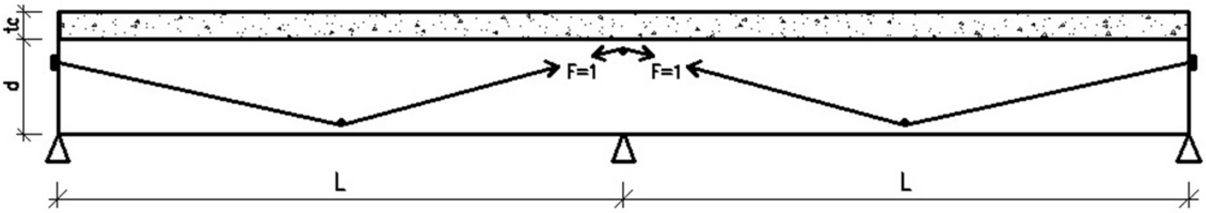

Figure 18. Unitary Force in the Tendons – Virtual Work Method

The compatibility of deformations in the central support is given by the Eqs. (15) to (17):

$$.\delta_{10} + \Delta F_p . \delta_{11} = 0 \tag{15}$$

$$.\delta_{10} = 2\int_0^L \frac{M.m}{E.I_{Long}} dx \tag{16}$$

$$.\delta_{11} = 2\left(\int_0^L \frac{m.m}{E.I_{Long}} dx + \int_0^L \frac{N_1.N_1}{E_p.A_p} dx + \int_0^L \frac{N_1.N_1}{E.A_{Long}} dx\right) \tag{17}$$

In which:

δ_{11} - displacement at the central bearing support generated by the unitary force of the tendons;

δ_{10} - displacement in the central bearing support generated by the external force (unitary negative moment in the support);

M - bending moment of the external loads (unit moment load in the internal support);

m - bending moment due to the unit force on the tendons;

N_1 - axial force due to unit force on the tendons;

A_p - cross-sectional area of the prestressing tendons;

I_{Long} - moment of inertia of the Long Term Composite Section Phase;

A_{Longa} - cross-sectional area of the Long Term Composite Section Phase.

Thus, by operating the Eqs. (11) and (12) for the yielding of top flange situation in ULS:

$$.M_d(LN) = \frac{F_{p\infty}.e + \frac{F_y}{d-LN}.I_{xt}(LN) + \frac{T_c(LN)}{LN}.I_{xc}(LN)}{1-\Delta F_p.e} \tag{18}$$

$$.F_H(LN) = \frac{F_y}{d-LN}.S_{xt}(LN) + F_{p\infty} + \Delta F_p.M_d(LN) - \frac{T_c(LN)}{LN}.S_{xc}(LN) \tag{19}$$

By using the same criterion for the compression bottom flange in ULS:

$$.M_d(LN) = \frac{F_{p\infty}.e + \frac{F_{nc}}{LN}.I_{xc}(LN) + \frac{T_t(LN)}{d-LN}.I_{xt}(LN)}{1-\Delta F_p.e} \tag{20}$$

$$.F_H(LN) = \frac{T_t(LN)}{d-LN}.S_{xt}(LN) + F_{p\infty} + \Delta F_p.M_d(LN) - \frac{F_{nc}}{LN}.S_{xc}(LN) \tag{21}$$

Likewise, if the tendons forcee [$F_{p\infty}$ + $\Delta F_p.M_d$ (LN)] exceeds its yielding limit, its force/stress will be given by:

$$.M_{de}(LN) = \frac{\left[f_{pyd}.A_p + \left(\frac{f_{pd}-f_{pyd}}{\varepsilon_u-\varepsilon_{yp}}\right).\left(\frac{F_{p\infty}}{E_p} - \varepsilon_{yp}.A_p\right)\right].e + \frac{T_t(LN)}{d-LN}.I_{xt}(LN) + \frac{F_{nc}(LN)}{LN}.I_{xc}(LN)}{1-\left(\frac{f_{pd}-f_{pyd}}{\varepsilon_u-\varepsilon_{yp}}\right).\Delta F_p.\frac{e}{E_p}} \quad (22)$$

$$.F_H(LN) = \frac{T_t(LN)}{d-LN}.S_{xt}(LN) + \left[f_{pyd} + \left(\frac{f_{pd}-f_{pyd}}{\varepsilon_u-\varepsilon_{yp}}\right).\left(\frac{F_{p\infty}+\Delta F_p.M_{de}(LN)}{E_pA_p} - \varepsilon_{yp}\right)\right] - \frac{F_{nc}}{LN}.S_{xc}(LN) \quad (23)$$

In which:

I_{xt}, I_{xc} – moments of inertia of the tensile and compression sections to LN;

S_{xt}, S_{xc} – static moments of the tensile and compression sections to LN;

M_d(LN) - strength negative moment, depending on the LN position;

F_H(LN) - horizontal forces sum, depending on the LN position;

$f_{pyd} = f_{pyk}/1.15 \rightarrow \varepsilon_{yd} = f_{pyd}/E_p$ ($f_{pyk} = 0.9f_{ptk}$; nominal yield stress of the strands);

$f_{pd} = f_{ptk}/1.15$ (f_{ptk} – nominal ultimate tensile stress of the strands);

ε_u = 35‰ – ultimate strain of the strands;

E_p, A_p – prestressing steel modulus of elasticity and area, respectively.

The strength bending moment is the smaller of the two (M_{de} or M_d). Thus, both the horizontal balance of forces and the strength bending moment (M_d) depend on the position of the Elastic Neutral Axis (NL); some iterative numerical method is required for the solution, such as Newton-Raphson or Bisection. In this work the Bisection method was used, which with 10 iterations already provides good results with errors of the order of 0.8%.

2.4 Reduced Bending Shear Effort

The prestressing effect is opposed to the external shear forces acting on the structure, as shown in Fig. 19.

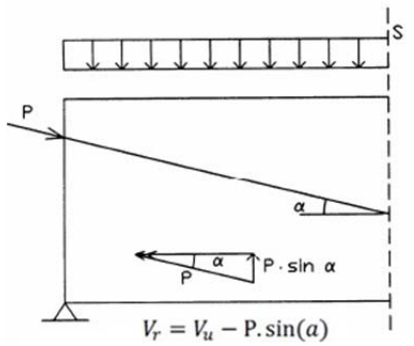

Figure 19. Relief of Shear Efforts by Prestressing

Thus, the ultimate shear stress (V_u) is reduced by the prestressing force. The calculation is done for each section, taking into account the tendons slope.

2.5 Results

The prestressing losses took into account the following effects: friction, wedge retreat, elastic shortening of the section, creep, shrinkage and prestressing strands relaxation. The calculations were implemented in MathCad and resulted in an average loss for the 4 tendons of 14.5%. The initial estimate of 15% is therefore consistent. At the end of the losses, each tendon should have a final force ≈ 273tons (total for 4 tendons ≈ 1090ton).

There was a 36.32% reduction in dead loads displacements at the center of the spans (from 4.02cm to 2.56cm) and 32.10% in live loads displacements (from 4.52cm to 3.07cm).

Using the Virtual Work Method, a relation was obtained between the negative bending moment in the central bearing support section and the additional force in the set of tendons. For each M = 1ton.m (10kN.m) there is a force increment in the tendons set of ΔF_p = 0.01667ton (0.167kN). Thus, it was possible to reach the ultimate plastic horizontal forces equilibrium in the support region by the Bisection method (see Eqs. 18 to 23).

Figure 20 shows the Strength Bending Moments without prestressing (Mn_P0), with prestressing (Md_Protende) and their ratio (Razão). Figure 21 presents the comparison between the Final Strength Prestressing Bending Moments and the Design Moments.

Mn_P0 = (kN·m)

	0
0	39630
1	39630
2	39390
3	43720
4	43720
5	43720
6	43720
7	43720
8	-12370
9	-13880
10	-14570

Md_Protende = (kN·m)

	0
0	41076
1	40056
2	39389
3	45433
4	45383
5	45610
6	46113
7	46887
8	-15957
9	-18218
10	-20506

Razão = (·%)

	0
0	3.65
1	1.07
2	0
3	3.92
4	3.8
5	4.32
6	5.47
7	7.24
8	28.99
9	31.25
10	40.74

Figure 20. Strength Bending Moments Comparison

Mumax = (kN·m)

	0
0	4910
1	9400
2	12920
3	14370
4	14410
5	13040
6	10320
7	6260
8	-4490
9	-9790
10	-17000

Md_Protende = (kN·m)

	0
0	41076
1	40056
2	39389
3	45433
4	45383
5	45610
6	46113
7	46887
8	-15957
9	-18218
10	-20506

Figure 21. M_{umax} (Design Moments Envelope) $M_{d\_Protende}$ (Prestressing Strength Bending Moments)

Therefore, it can be seen that, there is little gain in strength capacity in positive bending moment region (maximum increase of 7.24%). In the negative moment region, using the ULS criteria defined in the AASHTO-LRFD: 2012 standard, a significant increase of the strength capacity on the central support is obtained (40.74%).

The shear efforts were reduced by at least 25% (central support). Since the webs are responsible for shear strength capacity, a thickness reduction of the webs to 12.7 mm over the entire span length, would already guarantee the Ultimate Limit State. Which represents economy in steel (Fig. 22).

Vu = (kN)

	0
0	2000
1	1630
2	1090
3	990
4	840
5	1300
6	1770
7	2250
8	2730
9	3250
10	3600

Vr = (kN)

	0
0	2000
1	1038
2	498
3	398
4	250
5	706
6	879
7	1359
8	1844
9	2364
10	2711

Razão = (%)

	0
0	0
1	36
2	54
3	60
4	70
5	46
6	50
7	40
8	32
9	27
10	25

Figure 22. V_u (Design Shear Forces); V_r (Shear Strength Capacity after Prestressing); Razão (Ratio)

3 FINITE ELEMENTS MODEL

A Finite Elements Model is performed with the aid of the software SAP2000, in order to confront the results from the space frame bars model analysis from STRAP 2013. This comparison will be made in terms of displacements in state limit of service.

3.1 Definitions

A Finite Elements Model is performed in the software SAP2000 to confirm the analysis from the space frame bars model from STRAP 2013.

This model in SAP2000 was assembled from shell elements and space frame bar elements. For the slabs, four-node Reissner-Mindlin Thick Shell elements, fck = 40MPa (E_c = 38251MPa) were considered. For the other steel plates, from the box steel section (webs, flanges, stiffeners), four-node Kirchoff Shell-Thin elements and E_s = 200GPa were defined. The shear connectors were modeled with steel space frame bar elements of circular section with diameter Φ22,2mm and E_s = 200GPa.

The prestressing force was considered as an eccentric load inside the box section, following the eccentricities defined in Fig. 14, therefore it does not participate in the structure global stiffness. For the prestressing anchorage, it was necessary, due to the high stress concentration, to define transverse and longitudinal stiffening plates at the section heads (see Fig. 23). These plates were modeled with 32mm thick Kirchoff shell elements.

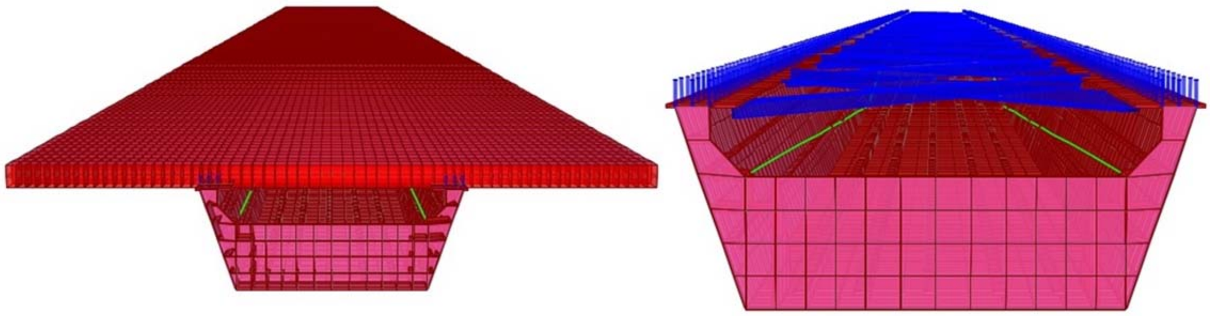

Figure 23. Finite Elements Method (FEM) Model

At the top flanges level of the box section, space frame bar elements 4 "x 4" # 3/8 " L-shaped were introduced for bracing the section (Fig. 23), mainly due loads g2 slabs dead loads and their torsion effect.

In the space frame bars model, the slab was homogenized and its width was divided by the ratio between materials Young Modulus. However, in the FEM model, this change would also modify the existence of nodes between the slab elements. Therefore, superposition of results would be inconsistent. In this way, it was decided to keep the slab width.

The definition of the mobile load was given by *dummy* bars positioned between the nodes of the slab elements. It is not possible to define, in SAP2000 as well as in STRAP 2013, a mobile load path directly on the element nodes, nor on the element areas, so the need for Dummy bars. Dummy bars do not have any permanent load and do not change the stiffness of the structure since their inertia is negligible.

3.2 Results

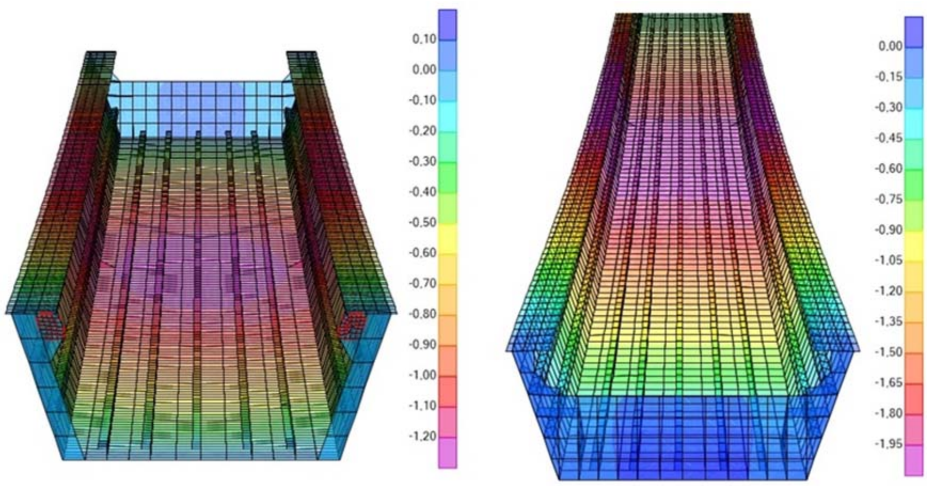

Figure 24. Strength Bending Moments Comparison

For the **Isostatic Box Section Phase**, the result for the space-frame bar model (SFBM) model provided displacement of 0.97cm in the center of the span of 25m. The FEM Model (Fig. 24 left) provides 17cm (20,62% higher). For load g2, **Hyperstatic Box Section Phase,** SFBM = -1.89cm; FEM Model = -1.98cm (Fig. 24 right) - 4.762% higher.

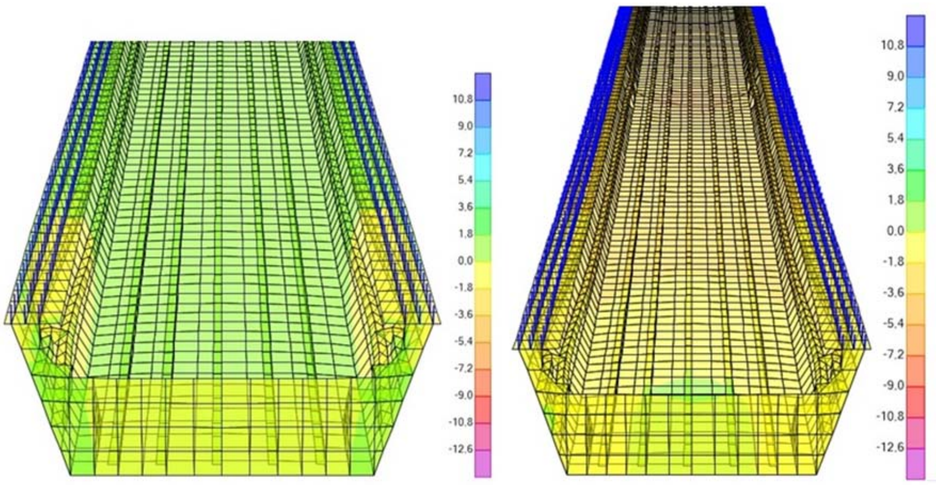

Figure 23. Strength Bending Moments Comparison

Long Term Composite Section Phase

For combination g3+prestressing (**Long Term Composite Section Phase**), the SFBM resulted + 0.965cm (span center), while the FEM Model, + 1.21cm (Fig. 23 left) - 25.38% higher. In the previous model (SFBM), the Service State Combinations Envelope provided maximum displacement in the span center of -3.07cm. For the same case, the FEM Model provides maximum displacement of -3.27cm (Fig. 23 right) - 6.515% higher.

4 CONCLUSIONS

The application prestressing force to the steel-concrete composite box girder bridges revealed a small positive bending moment increment (7.24%); Proving to be of little advantage, according to the AASHTO-LRFD:2012 criterion for the ULS. Maintaining the same criteria for ULS, the results showed a considerable increase strength negative bending moment (max. 40.74%); in this time, an important structural benefit is reached.

By the Virtual Work Method it was obtained the relation between the increase tendons force and the external negative bending moment on the central support (0.16673kN / kN.m). In contrast to the prestressed concrete, where there is deformation compatibility between strands and concrete, in this case, the force increase is connected to the bending moment. An iterative equations system is found for the horizontal balance and solved by the Bisection method.

Design Shear Forces were reduced by a minimum of 24.68%, reaching a maximum of 70% reduction. Thus, it would be possible to reduce the webs thickness to 12.7mm in ULS.

Shear connectors are verified / defined by the Fatigue Limit State, not by ULS.

The g3+prestressing load superposition as separate loads was possible in this case. For both SFBM and FEM Models, the analysis provides the coherent deformations/displacements for the situations: g3 + prestressing (isolated loads) and g3 + prestressing (in the same load case). Rigorously, a nonlinear analysis should be carried out when the prestressing load is defined, taking into account the tensions / deformations already existing in the structure and the geometrical and physical non-linearities from the previous loads.

ACKNOWLEDGEMENTS

I thank my family, my father Antonio Tadeu Velloso de Linhares and my mother Nilse Maria Tasca for all the affection, support and freedom they gave me.

I thank the Universidade Federal do Rio Grande do Sul (UFRGS) for the professional quality training that I had access to. I hope to contribute to its continuity.

I thank the Universidade Comunitária da Região de Chapecó (Unochapecó) for the opportunity to be part of its faculty, of which I feel very proud.

I make a special posthumous acknowledgment to my grandfather, Antonio Nelso Tasca, for inspiring in me the passion for knowledge.

REFERENCES

AMERICAN ASSOCIATION OF STATE HIGHWAY AND TRANSPORTATION OFFICIALS. **AASHTO-LRFD**: Bridge Design Specifications. Washington, 2012.

CHOI, D-H.; KIM, Y-S.; YOO, H. External post-tensioning of bridges by a rating equation considering the increment of a tendon force due to live loads. **Steel Structures**, v. 8, p. 109-118, 2008. Available in: < http://www.ceric.net/kssc/KSSC_3_2008_8_2_109(C).pdf >. Acess in: jun 5th 2014.

De NARDIN, S.; SOUZA, A. S. Sistema de vigas mistas contínuas e semicontínuas para edifícios. In: **XXXIII Jornadas Sudamericanas de Ingeniería Estructural**. Santiago de Chile : Escuela de Ingenieria Civil en Obras Civiles, 2008. p. 1-17.

DUAN, L; SALEH, Y.; ALTMAN, S. Steel-Concrete Composite I-Girder Bridges. In: CHEN, W.F.; DUAN, L. Bridge Engineering: Handbook. New York: CRC Press, 1999. p. 64/1-64/43.

KLAIBER, F.W.;WIPF, T.J. Strengthening and Rehabilitation. In: CHEN, W.F.; DUAN, L. Bridge Engineering: Handbook. New York: CRC Press, 1999. p. 50/1-50/42.

NUNZIATA, V. Prestressed steel structures. (Structture in acciaio precompresso). In: CONGRESSO C.T.A., XVII, 1999, Napoli. **Proceedings…** Napoli:[s.n.], 1999. p. 10. Available in: < http://www.studionunziata.com/sommario/memorie.htm>. Acess in: jun 15th 2014.

QUINAZ, C. M. da S. **Estruturas de aço e mistas pré-esforçoadas.** 1993. f. 236. Dissertação (Mestre em Estruturas de Engenharia Civil) – Faculdade de Engenharia da Universidade do Porto, Departamento de Engenharia Civil, Junho, 1993. Available in: <repositorio-aberto.up.pt/bitstream/10216/.../2/Texto%20integral.pdf>. Acess in: set. 19th 2014.

SALEH, Y.; DUAN, L. Steel-Concrete Composite Box Girder Bridges. In: CHEN, W.F.; DUAN, L. **Bridge Engineering**: Handbook. New York: CRC Press, 1999. p. 13/1-13/24.

SHIM, C. S.; CHUNG, C. H.; KIM, I. K.; KIM, Y. J. Innovative Prefabricated Composite Bridges. **Structural Engineering International:** International Association for Bridge and Structural Engineering (IABSE), Zurich, v. 20, n. 2, p. 126-133, May 2010.